Journal of the Physical Society of Japan **86**, 011009 (2017)
https://doi.org/10.7566/JPSJ.86.011009

THz Emission Spectroscopy for THz Spintronics

Thomas Jarik Huisman and Theo Rasing*

Radboud University, Institute for Molecules and Materials, 6525 AJ Nijmegen, The Netherlands

(Received October 1, 2016; accepted October 24, 2016; published online December 14, 2016)

Spintronics is used as the standard for the readout of magnetically stored data and also has commercial applications for writing data. The generation, control and detection of spin-polarized currents, spin-dependent electric transport, and pure spin currents on the subpicosecond (10^{-12} s) timescale are the next challenges in spintronics. Terahertz (THz, 10^{12} Hz) emission spectroscopy has proven to be an excellent tool for investigating these challenges. In this short review, we outline the functioning of this spectroscopic technique and its recent applications to spintronics.

1. Introduction

The seminal observation of subpicosecond light-induced demagnetization in ferromagnetic nickel two decades ago[1] can be considered as a key breakthrough towards ultrafast spintronics. The ultrafast laser-induced magnetization dynamics in magnetic metallic materials is mainly explained by laser-induced heating, i.e., light from the laser is absorbed by the electrons and, as a consequence, induces demagnetization. This laser-induced heating goes beyond the classical heating of a ferromagnet in a thermodynamical approach as it occurs on a subpicosecond timescale in which there is no thermodynamical equilibrium between the electrons, spins, and lattice.[2] The potential of ultrafast magnetization dynamics is evident for spintronics, especially for the commonly used metallic spintronics. However, as is shown in Fig. 1, laser-induced magnetization dynamics in metallic materials is likely to be accompanied by conductivity or even current dynamics, which are all potentially interesting for realizing ultrafast spintronics.[3]

As typical electronic transport measurements based on the application of electronic contacts can hardly reach a sub-100 ps time resolution,[4] optical techniques are mostly exploited for resolving ultrafast dynamics. A pump–probe approach is most commonly used, in which an intense short pulse stimulates (pumps) the dynamics and weak pulses monitor (probe) these dynamics. However, the applicability of this technique to distinguish the different possible types of dynamics is a topic causing a lot of controversy and discussion in the scientific community.[2,5–10] For instance, it was noticed that at the subpicosecond time scale, magneto-optical probes cannot always distinguish laser-induced changes to the magnetization and permittivity from each other.[11,12]

Alternatively, in order to deduce information about subpicosecond dynamics of the magnetization, one can employ the fact that such dynamics is accompanied by the emission of electromagnetic radiation at THz frequencies.[13,14] While this THz emission technique may also suffer from non-idealities, such as the dynamics of the dielectric permittivity, the model for the interpretation of the experimental results is more robust than that in the case of pump–probe techniques.[15] The recent demonstrations of ultrashort-laser-induced currents via spin–orbit coupling using only THz emission spectroscopy,[16–19] shows the potential applicability of this technique for developing ultrafast spintronics.

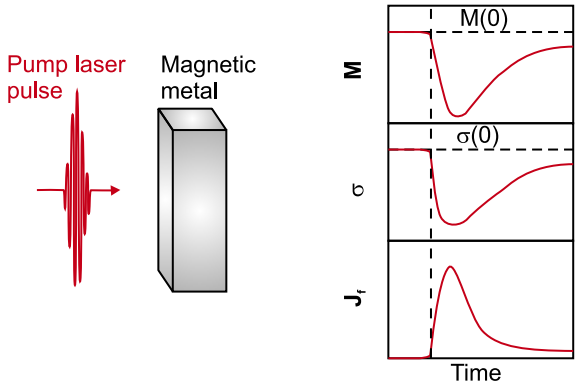

Fig. 1. (Color online) An intense laser pulse, called the pump, can induce ultrafast magnetization dynamics (**M**), current dynamics ($\mathbf{J}_f$), and changes to the conductivity (σ) of a magnetic metal. The vertical dashed line in the graphs indicates the moment at which the pump pulse as above arrives at the sample.

2. Generation and Detection of THz Emission

2.1 THz emission from the Maxwell equations

The source of THz emission can be written as a current. Combining Faraday's law

$$\nabla \times \mathbf{E} = -\frac{\partial \mathbf{B}}{\partial t} \tag{1}$$

with Ampère's law

$$\nabla \times \mathbf{B} = \mu_0 \mathbf{J} + \mu_0 \epsilon_0 \frac{\partial \mathbf{E}}{\partial t} \tag{2}$$

results, in the absence of static charges, in the wave equation:

$$\nabla^2 \mathbf{E} - \mu_0 \epsilon_0 \frac{\partial^2 \mathbf{E}}{\partial t^2} = \mu_0 \frac{\partial}{\partial t} \mathbf{J}, \tag{3}$$

where **E** is the electric field, ϵ_0 is the vacuum permittivity, μ_0 is the vacuum permeability, and **J** is the current density. Note that the current density can be written as

$$\mathbf{J} = \mathbf{J}_f + \nabla \times \mathbf{M} + \frac{\partial \mathbf{P}}{\partial t}, \tag{4}$$

where $\mathbf{J}_f$ is the free-current density, **M** is the magnetization, and **P** is the polarization. Combining this with the wave equation and writing it as a function of frequency rather than time gives us

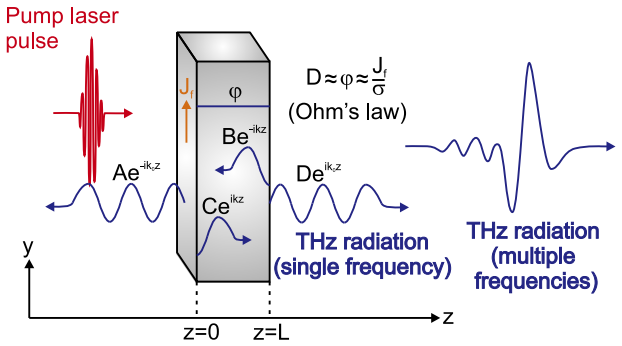

Fig. 2. (Color online) An intense laser pulse, called the pump, induces current dynamics ($\mathbf{J}_f$, drawn only at one surface), which subsequently emits radiation. The homogeneous and particular solutions of the wave equation for the electric field are shown with blue lines.

$$\nabla^2\mathbf{E} + \omega^2\mu_0\epsilon\mathbf{E} = \mu_0 i\omega[\mathbf{J}_f + \nabla \times \mathbf{M}], \tag{5}$$

with ϵ being the permittivity and ω the angular frequency. This wave equation shows that the electric field is coupled to the current density and magnetization via a differential equation with respect to space. Hence, the homogeneous and particular solutions of this differential equation for an electric field, show how THz radiation can be generated.

As an example of THz emission, we consider a slab of a material with coordinates as shown in Fig. 2. We assume that a laser induces homogeneous free-current dynamics along the y-axis at THz frequencies but no magnetization dynamics. As the wave equation is a linear differential equation, the resulting emission is at THz frequencies. The resulting electric field polarized parallel to the y-axis can be represented as

$$\tilde{E}_y(z) = \begin{cases} Ae^{-ik_0z} & z < 0 \\ Be^{-ikz} + Ce^{ikz} + \varphi & 0 < z < L \\ De^{ik_0z} & z > L \end{cases}, \tag{6}$$

where φ is a particular solution, k_0 is the wave vector in air, k is the wave vector in the slab and L is the thickness of the slab. The emitted electric fields are represented by Ae^{-ik_0z} and De^{ik_0z}, where in practice De^{ik_0z} is commonly measured as it is along the propagation direction of the incident light. Taking φ as a constant with respect to z, we find from Eq. (5) that $\varphi = \frac{i}{\omega\epsilon}\mathbf{J}_f$. Furthermore, for metals, it is reasonable to take $\epsilon \approx \frac{i}{\omega}\sigma$ with σ being the conductivity, such that $\varphi = \frac{\mathbf{J}_f}{\sigma}$, which is exactly Ohm's law. By assuming the electric field and the derivative of the electric field to be continuous across the interfaces, we can formulate the following boundary conditions:

$$\begin{cases} A = B + C + \varphi & z = 0 \\ -k_0A = -kB + kC & z = 0 \\ Be^{-ikL} + Ce^{ikL} + \varphi = De^{ik_0L} & z = L \\ -kBe^{-ikL} + kCe^{ikL} = k_0De^{ik_0L} & z = L \end{cases}. \tag{7}$$

Equation (7) is a set of four equations with four variables, from which we can extract the emission amplitude as

$$De^{ik_0L} = -\varphi\frac{k(e^{ikL} - 1)}{k + k_0 + (k_0 - k)e^{ikL}}. \tag{8}$$

When working with thin metallic layers and at THz frequencies, we can consider the low-thickness limit ($kL \ll 1$) and the metallic limit ($k \gg k_0$), such that

$$D \approx \varphi \approx \frac{\mathbf{J}_f}{\sigma}. \tag{9}$$

Hence, the emitted amplitude at these limits is given by Ohm's law. Since THz emission can be measured on a sub-picosecond time scale, THz emission spectroscopy may be regarded as an ultrafast ammeter, within limits such as the ones just mentioned. Similarly, for ultrafast magnetization dynamics, the THz emission spectroscopy may in some cases be regarded as an ultrafast magnetometer.

2.2 *THz detection*

The most common way to detect THz emission with ultrashort laser pulses is by optical gating.[20] The optical gating technique can be achieved either by using a photoconductive antenna or via nonlinear optical methods.[21] The nonlinear optical methods, also known as electro-optic sampling, typically rely on the Pockels effect, in which the refractive index of a material depends on a static or slowly varying electric field.[22] Hence, when the optical probe pulses arrive simultaneously with the THz radiation, the electric field of the THz radiation can modify the refractive index of a nonlinear optical crystal $n(E_{THz})$ and thereby introduce birefringence to the probe pulses. The amount of ellipticity gained by the probe pulses is directly proportional to the amplitude of the electric field of the THz radiation. By varying the difference in the arrival time between the THz radiation and the probe pulses at the material while measuring the ellipticity of the probe pulses [see also Fig. 3(a)], we can reconstruct the electric field of THz radiation in time. An example of an electric field measured from laser-induced magnetization dynamics in a magnetically ordered film is shown in Fig. 3(b). By using the Fourier transformation, we obtain the corresponding spectrum, also shown in Fig. 3(b).

Using a photoconductive antenna, the optical pulses are absorbed through an interband transition in a semiconductor in order to produce charge carriers. Subsequently, the electric field of the THz radiation drives these charge carriers to form a current, which is typically collected using a metallic antenna structure on top of the semiconductor. The amplitude and direction of the resulting current are determined by the amplitude and direction of the electric field at the time of overlap with the optical pulses. Similar to the electro-optic sampling technique, we vary the difference in the arrival time between the optical and THz pulses at the antenna in order to reconstruct the electric field of the THz radiation in time.

2.3 *THz emission from sample to detector*

Once the THz radiation is generated from the sample, it will typically follow Gaussian wave propagation.[23] This commonly means that the THz radiation is diffraction-limited near the sample and diverges as it propagates away from the sample. To collect and refocus the THz radiation onto the detector, either lenses or metallic parabolic mirrors can be used. Owing to the finite aperture of these focusing optics, the lower frequencies will be more attenuated, with DC signals being fully attenuated, owing to their stronger

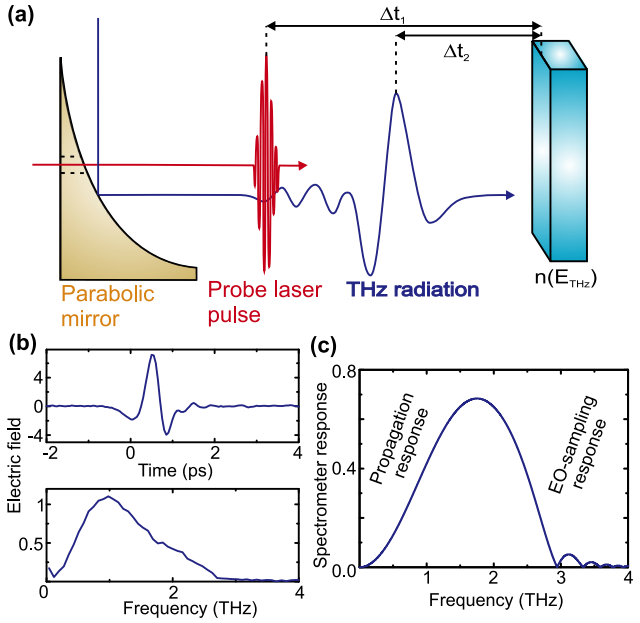

Fig. 3. (Color online) (a) With electro-optic sampling, the electric field of THz radiation modifies the optical properties of a material $n(E_{THz})$, which may result in THz-induced ellipticity of the probe pulses. By varying the difference in the arrivel time between the THz radiation and the optical pulses at the material $(\Delta t_2 - \Delta t_1)$ while monitoring the electric-field-induced changes to the optical probe, we can reconstruct the electric field of THz radiation in time. Parabolic mirrors with a small hole are commonly used in order to overlap the laser pulses and THz radiation, and to focus the THz radiation onto the nonlinear crystal used for detection. (b) Example of the measured electric field as a function of time. By Fourier transformation we obtain the corresponding spectrum. (c) Example of the spectrometer response, i.e., the efficiency with which certain frequencies are measured. This response is attenuated for low frequencies due to the propagation of radiation, while high frequencies are attenuated by the electro-optic (EO) sampling response. Figures adapted from Ref. 15.

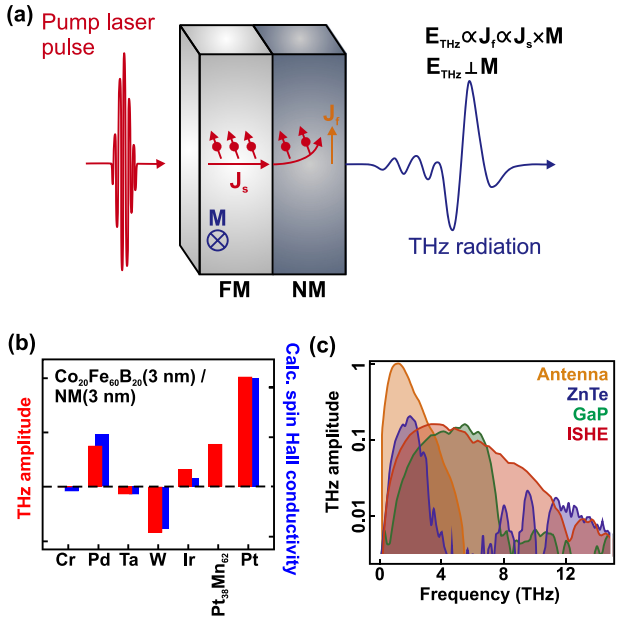

Fig. 4. (Color online) (a) An ultrashort laser pulse initiates the injection of spin-polarized electrons ($\mathbf{J}_s$) from a ferromagnetic metallic layer (FM) into a nonmagnetic metallic layer (NM). Subsequently, the inverse spin Hall effect (ISHE) causes the path of these electrons to deviate, creating a charge current ($\mathbf{J}_f$) in the plane of the sample. This charge current can give rise to the emission of THz radiation. (b) Comparison of the measured THz emission amplitude with the ISHE conductivity for different NM materials. (c) Comparison of the measured THz emission spectra using the ISHE and other commonly used THz emitters. Adapted with permission from Ref. 18.

divergence. On the other hand, the propagation from the sample to the detector allows the implementation of polarizers, allowing polarization-resolved measurements of the THz emission without the need for a polarization-sensitive detector.

The attenuation of lower frequencies due to the propagation losses in combination with the response of the optically gated detection determine the spectrometer response. An example of this spectrometer response is shown in Fig. 3(c). In practice, the optically gated detection response often limits the upper-frequency response, which for instance, for the commonly used ZnTe crystals is slightly above 3 THz.[24] By a ZnTe crystal of μm-order thicknesses, or by using a different material, this frequency limit can be improved, but usually there is a trade-off with the detection sensitivity.

3. THz Emission from THz Spintronics

3.1 Ultrafast inverse spin Hall effect

It was proposed that illuminating a ferromagnetic metal layer with ultrashort laser pulses creates hot electrons, which move in random directions with velocities depending on the spin direction.[9] In this way, it is possible to inject spin-polarized electrons into an adjacent metallic layer on a sub-picosecond timescale. If this adjacent layer has a strong spin–orbit coupling, the inverse spin Hall effect[25] can subsequently cause the path of these spin-polarized electrons to deviate depending on their spin direction, as shown in Fig. 4(a).

This two-step process, in which light first generates out-of-equilibrium electrons, which subsequently create a charge current in the adjacent layer, was first demonstrated using THz emission spectroscopy in Ref. 16. This study showed that using laser pulses with a repetition rate of 1 kHz, a wavelength of 800 nm, a width of 10 fs order, and a pulse energy of about 1 mJ/cm^2, laser-induced THz emission could be observed in metallic bilayers by using electro-optic sampling in a 250-μm-thick GaP crystal. Using comparable experimental approaches, Refs. 17–19 recently repeated and extended studies on THz emission from metallic heterostructures using various metallic layers with thicknesses of nm order. These works show that the sign of the THz emission is fully determined by both the magnetization direction of the ferromagnetic layer and the order of growth of the bilayer structure. The latter is of special importance as it excludes the possibility that the emission solely originates from laser-induced magnetization dynamics in the ferromagnetic layer.[15] Thereby, it was shown that the amplitude of the emitted radiation scales with the spin–orbit coupling strength of the capping layer [see also Fig. 4(b)].

Not only are these results a clear push towards ultrafast spintronics, Fig. 4(c) shows that the generation efficiency and bandwidth of the emitted THz radiation are also very high compared with those of commonly used THz emitters.[18] The amplitude of the emission appears to be of the same order of magnitude as that of standard emitters, while the measurable bandwidth can span about 30 THz, which is in some cases an order of magnitude higher than that produced by standard

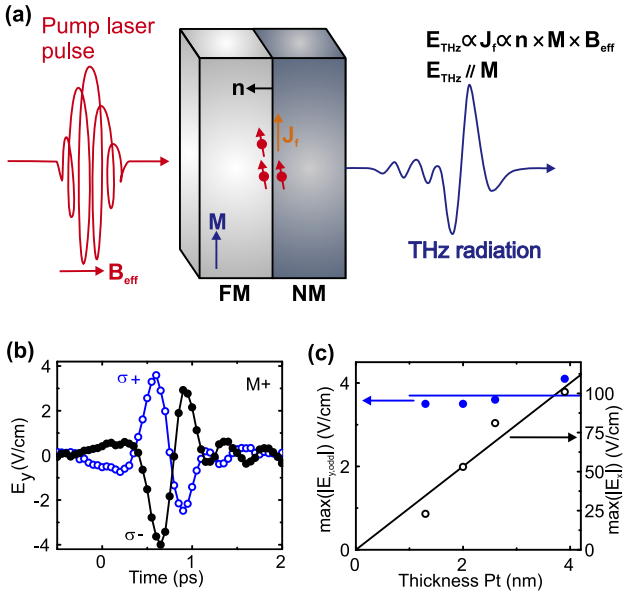

Fig. 5. (Color online) (a) An ultrashort circularly polarized laser pulse acts as an effective magnetic field ($\mathbf{B}_{\text{eff}}$) in the magnetization of a ferromagnetic metallic layer (FM). Subsequently, spin–orbit coupling from the non-magnetic metallic layer (NM) near the interface transforms the magnetization dynamics into current dynamics ($\mathbf{J}_{\text{f}}$) in the plane of the sample. This charge current can induce the emission of THz radiation. (b) Measured THz emission as a function of time for opposite helicities of the pump pulses. M+ indicates that the magnetization is saturated in a fixed direction. (c) Amplitudes for the Rashba ($E_{y,\text{odd}}$), and ISHE (E_x) mediated THz emission as a function of the thickness of a platinum NM layer. Figures adapted from Ref. 17.

emitters. Furthermore, Ref. 19 shows that by using repeated multilayer stacks separated by a thin insulating layer, the amplitude of THz emission can be further increased to about 50%.

3.2 *Ultrafast polarization-controlled spintronics*

Moreover, Ref. 17 showed that using a similar experimental approach and metallic bilayers in which the ferromagnetic layer is 10-nm-thick Co, a light-induced current could be generated whose direction is not only given by the growth order and magnetization direction but also by the polarization of the incident light. Whereas a polarization-independent current was directed perpendicular to the magnetization direction of the ferromagnet, a polarization-dependent current was observed directed parallel to the magnetization direction. As shown in Fig. 5(a), a circularly polarized laser pulse was used to induce this polarization-dependent current.

The inspiration for this polarization-dependent effect came from demonstrations of the generation of electrical photocurrents with the help of the spin–orbit interaction and circularly polarized light in semiconductors.[26] It is known that circularly polarized light can act as an effective magnetic field ($\mathbf{B}_{\text{eff}}$) parallel to the propagation direction of light via the non-dissipative inverse Faraday effect[27,28] or due to the dissipative optical spin transfer torque effect,[29] which can act as a torque on the magnetization such that it starts to tilt ($\mathbf{M}^* \propto [\mathbf{M} \times \mathbf{B}_{\text{eff}}]$). Subsequently, spin–orbit coupling with a Rashba symmetry may provide a current represented by $\mathbf{J} \propto \mathbf{n} \times [\mathbf{M} \times \mathbf{B}_{\text{eff}}]$, where $\mathbf{n}$ is the direction of inversion symmetry breaking. While the required spin–orbit coupling in the works on semiconductors is provided by spatial inversion symmetry breaking, also known as the Rashba effect, metals are typically centrosymmetric. However, at the interfaces of metallic layers there is breaking of spatial inversion symmetry, making it possible to use the described approach to generate a photocurrent via spin–orbit coupling. Indeed, electronic transport measurements also deem the Rashba effect in a metallic bilayer to be significant.[30] Reference 17 shows that the sign of THz emission polarized parallel to the magnetization from metallic bilayers is determined by the helicity of light [see Fig. 5(b)], the magnetization direction of the ferromagnet, and the direction of the inversion symmetry breaking, as expected from a Rashba-mediated effect.

By measuring the emission as a function of the thickness of the non-magnetic layer and for different nonmagnetic layers, it is shown that the polarization-dependent and -independent emissions (with orthogonal polarizations) are not obviously correlated, except for a tendency for the amplitude to increase with increasing strength of the spin–orbit coupling. Whereas the polarization independent emission is attributed to spin-diffusion with the inverse spin Hall effect subsequently generating a current, the polarization-dependent emission is attributed to a tilt of the magnetization and the interfacial Rashba effect causing the generation of a current. The most pronounced observation indicating an interfacial effect is the fact that the helicity-dependent photocurrent seems to be hardly dependent on the thickness of the nonmagnetic layer, while the polarization-independent emission clearly is dependent, as shown in Fig. 5(c). Furthermore, from the fluence dependence, a two-step process in which the intensity of light excites hot carriers before or after a helicity dependent interaction takes place can be excluded for the helicity dependent photocurrent.[17]

The generation of ultrashort current pulses using light that depend on the magnetization shows that a slow voltage source may be replaced with ultrashort laser pulses for ultrafast spintronics. The control over the direction of this current via the polarization of light, moreover shows the potential for ultrafast control. However, the polarization-dependent currents were found to be one or two orders of magnitude weaker than the polarization-independent currents. This may change when the polarization independent current is suppressed by using thinner layers while the interfacial polarization dependent current remains unaffected.

4. Prospects for the Near Future

As the potential of THz emission spectroscopy for THz spintronics has only been recently discovered, we can expect to see many more investigations in this direction. Reference 18 shows an example of a more extended structure than a bilayer, i.e., a trilayer, which can provide higher emission amplitudes. Another implementation of a trilayer could be by inserting a spacer layer in a bilayer structure. If this seperation layer is conducting and without significant spin–orbit coupling, we may expect to significantly alter the interfacial effects while maintaining the spin-diffusion-mediated mechanisms to some extend.

Alternatively, antiferromagnetic spintronics have also recently emerged as having potential for future spintronic devices.[31] Attractive features of antiferromagnetic spin-

tronics include insensitivity to disturbing magnetic fields, no disturbing interactions between neighboring antiferromagnetic elements, and intrinsically faster spin dynamics than ferromagnets. Together with the fact that THz emission spectroscopy has already been succesfully applied to (canted) antiferromagnets,[32,33] it is very likely that attempts will be made for measuring spin(-polarized) currents from an antiferromagnet.

From the viewpoint of THz transmission spectroscopy, several developments may also be expected. A spintronic emitter based on the inverse spin Hall effect shows very promising characteristics and is easily accessible. When combined with a broadband detector, perhaps in the future also based on spintronics, it may provide a state-of-the-art bandwidth. Furthermore, the low coercive fields of these spintronic emitters allows for magnetic modulation, which can be used as a polarization modulation scheme and which would be an excellent alternative for the currently used mechanically demanding polarization modulation schemes.[34,35]

Acknowledgments

We thank Alexey Kimel for fruitful discussions. This work was supported by the Foundation for Fundamental Research on Matter (FOM), the European Union's Seventh Framework Program (FP7/2007-2013) grant No. 280555 (Go-Fast) and grant No. 281043 (FemtoSpin), European Research Council grant No. 257280 (Femtomagnetism) and grant No. 339813 (Exchange).

*th.rasing@science.ru.nl

1) E. Beaurepaire, J.-C. Merle, A. Daunois, and J.-Y. Bigot, Phys. Rev. Lett. **76**, 4250 (1996).
2) A. Kirilyuk, A. V. Kimel, and Th. Rasing, Rev. Mod. Phys. **82**, 2731 (2010).
3) J. Walowski and M. Münzenberg, J. Appl. Phys. **120**, 140901 (2016).
4) Z. Zhong, N. M. Gabor, J. E. Sharping, A. L. Gaeta, and P. L. McEuen, Nat. Nanotechnol. **3**, 201 (2008).
5) L. Guidoni, E. Beaurepaire, and J.-Y. Bigot, Phys. Rev. Lett. **89**, 017401 (2002).
6) J.-Y. Bigot, M. Vomir, and E. Beaurepaire, Nat. Phys. **5**, 515 (2009).
7) G. P. Zhang, W. Hübner, G. Lefkidis, Y. Bai, and T. F. George, Nat. Phys. **5**, 499 (2009).
8) B. Koopmans, G. Malinowski, F. Dalla Longa, D. Steiauf, M. Fähnle, T. Roth, M. Cinchetti, and M. Aeschlimann, Nat. Mater. **9**, 259 (2010).
9) M. Battiato, K. Carva, and P. M. Oppeneer, Phys. Rev. Lett. **105**, 027203 (2010).
10) K. Carva, M. Battiato, and P. M. Oppeneer, Nat. Phys. **7**, 665 (2011).
11) H. Regensburger, R. Vollmer, and J. Kirschner, Phys. Rev. B **61**, 14716 (2000).
12) B. Koopmans, M. van Kampen, J. T. Kohlhepp, and W. J. M. de Jonge, Phys. Rev. Lett. **85**, 844 (2000).
13) E. Beaurepaire, G. M. Turner, S. M. Harrel, M. C. Beard, J.-Y. Bigot, and C. A. Schmuttenmaer, Appl. Phys. Lett. **84**, 3465 (2004).
14) D. J. Hilton, R. D. Averitt, C. A. Meserole, G. L. Fisher, D. J. Funk, J. D. Thompson, and A. J. Taylor, Opt. Lett. **29**, 1805 (2004).
15) T. J. Huisman, R. V. Mikhaylovskiy, A. Tsukamoto, Th. Rasing, and A. V. Kimel, Phys. Rev. B **92**, 104419 (2015).
16) T. Kampfrath, M. Battiato, P. Maldonado, G. Eilers, J. Nötzold, S. Mährlein, V. Zbarsky, F. Freimuth, Y. Mokrousov, S. Blügel, M. Wolf, I. Radu, P. M. Oppeneer, and M. Münzenberg, Nat. Nanotechnol. **8**, 256 (2013).
17) T. J. Huisman, R. V. Mikhaylovskiy, J. D. Costa, F. Freimuth, E. Paz, J. Ventura, P. P. Freitas, S. Blügel, Y. Mokrousov, Th. Rasing, and A. V. Kimel, Nat. Nanotechnol. **11**, 455 (2016).
18) T. Seifert, S. Jaiswal, U. Martens, J. Hannegan, L. Braun, P. Maldonado, F. Freimuth, A. Kronenberg, J. Henrizi, I. Radu, E. Beaurepaire, Y. Mokrousov, P. M. Oppeneer, M. Jourdan, G. Jakob, D. Turchinovich, L. M. Hayden, M. Wolf, M. Münzenberg, M. Kläui, and T. Kampfrath, Nat. Photonics **10**, 483 (2016).
19) D. Yang, J. Liang, C. Zhou, L. Sun, R. Zheng, S. Luo, Y. Wu, and J. Qui, Adv. Opt. Mater. (in press) [DOI: 10.1002/adom.201600270].
20) R. Ulbricht, E. Hendry, J. Shan, T. F. Heinz, and M. Bonn, Rev. Mod. Phys. **83**, 543 (2011).
21) Y. Cai, I. Brener, J. Lopata, J. Wynn, L. Pfeiffer, J. B. Stark, Q. Wu, X. C. Zhang, and J. F. Federici, Appl. Phys. Lett. **73**, 444 (1998).
22) B. E. A. Saleh and M. C. Teich, *Fundamentals of Photonics* (Wiley, Hoboken, NJ, 2007) 2nd ed.
23) P. Kužel, M. A. Khazan, and J. Kroupa, J. Opt. Soc. Am. B **16**, 1795 (1999).
24) G. Gallot, J. Zhang, R. W. McGowan, T.-I. Jeon, and D. Grischkowsky, Appl. Phys. Lett. **74**, 3450 (1999).
25) J. E. Hirsch, Phys. Rev. Lett. **83**, 1834 (1999).
26) S. D. Ganichev, E. L. Ivchenko, V. V. Bel'kov, S. A. Tarasenko, M. Sollinger, D. Weiss, W. Wegscheider, and W. Prettl, Nature **417**, 153 (2002).
27) P. S. Pershan, J. P. van der Ziel, and L. D. Malmstrom, Phys. Rev. **143**, 574 (1966).
28) A. V. Kimel, A. Kirilyuk, P. A. Usachev, R. V. Pisarev, A. M. Balbashov, and Th. Rasing, Nature **435**, 655 (2005).
29) P. Němec, E. Rozkotová, N. Tesařová, F. Trojánek, E. De Ranieri, K. Olejník, J. Zemen, V. Novák, M. Cukr, P. Malý, and T. Jungwirth, Nat. Phys. **8**, 411 (2012).
30) I. Mihai Miron, G. Gaudin, S. Auffret, B. Rodmacq, A. Schuhl, S. Pizzini, J. Vogel, and P. Gambardella, Nat. Mater. **9**, 230 (2010).
31) T. Jungwirth, X. Marti, P. Wadley, and J. Wunderlich, Nat. Nanotechnol. **11**, 231 (2016).
32) R. V. Mikhaylovskiy, E. Hendry, A. Secchi, J. H. Mentink, M. Eckstein, A. Wu, R. V. Pisarev, V. V. Kruglyak, M. I. Katsnelson, Th. Rasing, and A. V. Kimel, Nat. Commun. **6**, 8190 (2015).
33) R. V. Mikhaylovskiy, T. J. Huisman, A. I. Popov, A. K. Zvezdin, Th. Rasing, R. V. Pisarev, and A. V. Kimel, Phys. Rev. B **92**, 094437 (2015).
34) C. M. Morris, R. Valdés Aguilar, A. V. Stier, and N. P. Armitage, Opt. Express **20**, 12303 (2012).
35) N. Yasumatsu and S. Watanabe, Rev. Sci. Instrum. **83**, 023104 (2012).

Thomas Jarik Huisman received his Masters in Applied Physics in 2012. Since 2013 he has been a Ph.D. candidate at Radboud University in the Institute for Molecules and Materials.

Theo Rasing received his Ph.D. from Nijmegen in 1982 on Incommensurate Crystals and worked at the University of California at Berkeley between 1982 and 1988. He is a full professor in experimental solid state physics at the Radboud University and the director of its Institute for Molecules and Materials.